Journal of Non-Newtonian Fluid Mechanics 290 (2021) 104508

Contents lists available at ScienceDirect

Journal of Non-Newtonian Fluid Mechanics

journal homepage: www.elsevier.com/locate/jnnfm

Polymer effects on viscoelastic fluid flows in a planar constriction microchannel

Sen Wu [a,b,1], Mahmud Kamal Raihan [b,1], Le Song [b,c], Xingchen Shao [d], Joshua B. Bostwick [b], Liandong Yu [c,e], Xinxiang Pan [a,f], Xiangchun Xuan [b,*]

[a] College of Marine Engineering, Dalian Maritime University, Dalian 116026, PR China
[b] Department of Mechanical Engineering, Clemson University, Clemson, SC 29634-0921 USA
[c] School of Instrument Science and Opto-electronic Engineering, Hefei University of Technology, Hefei 230009, PR China
[d] Department of Chemical and Biomolecular Engineering, Johns Hopkins University, Baltimore, MD 21218, USA
[e] College of Controlling Science and Engineering, China University of Petroleum, Qingdao 257061, PR China
[f] Maritime College, Guangdong Ocean University, Zhanjiang 524088, PR China

ARTICLE INFO

Keywords:
Polymer solutions
Elasticity
Shear thinning
Inertia
Microfluidic model
Porous media

ABSTRACT

A comprehensive understanding of the flow of viscoelastic polymer solutions in a contraction and/or an expansion geometry concerns numerous applications. The effects of polymer type, molecular weight, and concentration are investigated through controlled experiments with polyethylene oxide (PEO), polyvinylpyrrolidone (PVP) and hyaluronic acid (HA) solutions in a planar constriction microchannel in a wide range of Reynolds (Re) and Weissenberg (Wi) numbers. The polymer structure renders drastic differences amongst the contraction flows of 3000 ppm PEO, PVP, and HA solutions despite having similar molecular weights. The expansion flow vortices of these solutions remain analogous to those in the inertial flow of water. Increasing the molecular weight or concentration of PEO polymer promotes the elastic instabilities in both the contraction and expansion flows. It, however, suppresses (and even blocks) the inertial vortices in the expansion flow and makes them start from the salient corners, in contrast to the lips of the expansion walls in water. Interestingly, a sudden decrease in the size of inertial vortices is observed in the expansion flow of 500 ppm, 1 megadalton PEO solution when the elastic disturbances start appearing in the contraction flow. The observed flow regimes and vortex development in the polymer solutions are summarized in the same dimensionless $Re - Wi$ and $Re - \chi_L$ parameter spaces, where χ_L is the normalized vortex length. The elasticity number, $El = Wi/Re$, is found to determine and distinguish the contraction and expansion flows.

1. Introduction

Polymer structural dynamics in the flow of non-Newtonian fluids holds significance in many naturally and industrially occurring phenomena [1–3]. Depending on various inherent factors such as chain length, flexibility, entanglement, ionic strength and relaxation of the conformation, flow of polymer solutions can behave in different manners while running through passages having different forms and shapes [4–11]. These behaviors often dictate the desired outcome of the process, may it be fiber spinning [12–14], flow mixing [15–18], or particle separation in lab-on-a-chip devices [19–22]. The change in rheology due to the shift of the flow regime from shear to extensional also plays an important role in this regard since an abrupt alteration of shape along the channel is very common in such processes [23–28]. Hence, numerous studies have been conducted over the decades for a better grasp of the fluid rheological effects on the flow pattern through axisymmetric, planar or square contractions and/or expansions [29–48]. There have also been a number of investigations on the influence of the dimension and topology of the channel concerning the expansion/contraction ratio, aspect ratio, and length of the constriction [49–56]. The applications pertain to various analogous fields of flow through actual porous media such as enhanced oil recovery from unconventional reservoirs, inkjet printheads, industrial milling drag reducing practices, biological and chemical extraction and isolation

* Corresponding author.
E-mail address: xcxuan@clemson.edu (X. Xuan).
[1] These authors contributed equally to this work.

https://doi.org/10.1016/j.jnnfm.2021.104508
Received 24 December 2020; Received in revised form 18 February 2021; Accepted 20 February 2021
Available online 23 February 2021

processes, and environmental remediation methods [57–59].

Despite the importance, the influence of polymer structure at the molecular scale on the flow behavior at the micro/macroscale is a conundrum yet to be unraveled. The works of Daoud et al. [60], Graessley [61], and Rubenstein and Colby [62] have shed light on the significance of polymer structure on the rheology of neutral polymers. Charged polyelectrolyte solutions were investigated by Dobrynin and Rubinstein [63], which provides insight on the interaction of charge repulsion and counterion condensation. Methods such as changing the polymer concentration, adding salt to polyelectrolyte solutions to neutralize them, and mixing charged surfactants to neutral polymer solutions in order to have ions present, have been commonly used in recent studies to further comprehend the effects of polymer conformation in the channel flow phenomena. For example, Rodd et al. [64] studied the entry flow of polyethylene oxide (PEO) solutions through a micro-fabricated planar abrupt contraction-expansion. They demonstrated the strong influence of PEO concentration on the inertia-elastic flow development. Lanzaro et al. [65] observed chaotic-like flow patterns in a high-concentration polyacrylamide (PAA) solution while only symmetric corner vortices appeared in the low-concentration solution. Li et al. [66] reported the effect of (Patrick Knappe, 2010)polydispersity on the elastic properties of PEO solutions having different molecular weights, and in turn the evolution of vortex formation and stability with respect to the elasticity number. Miller and Cooper-White [67] investigated the transition of flow regimes in sodium dodecyl sulfate (SDS) surfactant added PEO solution that becomes shear thinning after aggregating with the anionic micelles. The effect of adding sodium salt to the PAA solution was studied by Campo-Deano et al. [68], where a change in the viscosity and shear thinning property was observed in the salt solution with different vortex development ensued. Other groups such as Kawale et al. [69] and Ekanem et al. [70] studied the salt effects on the flow of hydrolyzed PAA solution. In addition, Hidema et al. [71] found that the polymer entanglement has a stronger effect on the constriction flow than the relaxation time and polymer rigidity with hyaluronic acid (HA) sodium salt dissolved in water and phosphate buffer saline solution, respectively.

The existing works have enhanced the comprehension of polymer conformation under flow conditions, but further generalized studies concerning polymer structural properties are required in a single platform to directly compare their influences and hence unify and bring the results under the same roof. In a recent work, we have studied the fluid rheological effects on the flow of four types of polymer solutions including xanthan gum (XG), polyvinylpyrrolidone (PVP), PEO and PAA in a planar contraction-expansion microchannel [72]. These non-Newtonian fluids have dissimilar molecular weights and concentrations, leading to significantly different elastic and shear thinning properties. Their flows were compared among each other and also against that of Newtonian water in a similar wide range of flow rates in the same microchannel. It was found that fluid inertia and shear thinning are responsible for the vortex development in the expansion and contraction flows, respectively. However, we were unable to elucidate a definitive effect of fluid elasticity from the four polymer solutions that have significantly different polymer structures without a common ground.

This work is aimed to provide further experimental data on the fluid elasticity effects in the flow of polymer solutions through a planar constriction microchannel. We investigate the respective influences of polymer type, molecular weight and concentration by conducting controlled experiments with PEO, PVP and HA solutions. Each test is performed by varying only the parameter in question while keeping everything else fixed. The flow development is characterized using dimensionless numbers for the fluid elasticity, shear thinning, and inertia effects, respectively. Moreover, the observed flow regimes and vortex growth are compared in the same dimensionless parameter spaces for the purpose of elucidating the routine(s). Our findings in this work can be useful to various analogous systems, for instance, polymer interaction with brines during the oil recovery in porous media because a planar contraction-expansion structure is considered as one of the simplest laboratory models of actual pore-throat networks [28,59]. Moreover, our work can be used as the experimental data for numerical constitutive model improvements as well as microfluidic rheometry [73–75].

2. Experiment

2.1. Materials

Fig. 1 shows a picture of the planar abrupt contraction-expansion microchannel used in the experiment. The length and width of the main channel are 1 cm and 400 μm, respectively, with a uniform height of 55 μm. The constriction is in the middle of the channel with a width of 40 μm and a length of 200 μm. The microchannel was fabricated with polydimethylsiloxane (PDMS) using the standard soft lithography technique [76]. Three primary types of aqueous polymer solutions including PEO (Sigma-Aldrich, St. Louis, MI), PVP (Sigma-Aldrich, St. Louis, MI) and HA (Lifecore Biomedical LLC, Chaska, MN) were employed to investigate various polymer effects on the viscoelastic flow pattern in the constriction microchannel. For the effect of polymer type, we prepared 3000 ppm solutions of PEO [$M_w = 0.3$ megadalton (MDa)], PVP ($M_w = 0.36$ MDa) and HA ($M_w = 0.357$ MDa) polymers with similar molecular weights. DI water (Thermo Fisher Scientific, Waltham, MA) was also tested as the control experiment. For the effect of polymer molecular weight, we prepared 1000 ppm solutions of PEO polymer with the molecular weight ranging from 0.3 to 0.6, 1, 2 and 4 MDa. For the effect of polymer concentration, we diluted the original 5000 ppm solution of $M_w = 1$ MDa PEO polymer to 500, 1000, 1500, 2000 and 3000 ppm, respectively.

The dynamic viscosity of each of the prepared fluids was measured using a cone-plate rheometer (Anton Paar, MCR 302, Graz, Austria) at room temperature. The measured data for the shear rate ranging from 10 to 2,000 s^{-1} are shown in Fig. 2. Those viscosity data for the fluids exhibiting shear thinning behaviors are also curve-fitted using the Carreau model in order for a quantitative comparison of the power-law index, n [12],

$$\frac{\eta - \eta_\infty}{\eta_0 - \eta_\infty} = \left[1 + (\lambda_C \dot{\gamma})^2\right]^{(n-1)/2} \tag{1}$$

where, η_∞ is the infinite-shear-rate viscosity, η_0 is the zero-shear-rate

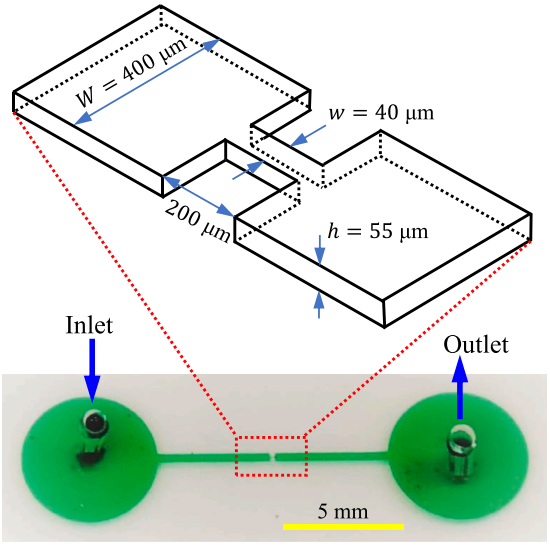

Fig. 1. Perspective view of the planar constriction microchannel with the inset showing the contraction-expansion region with dimensions.

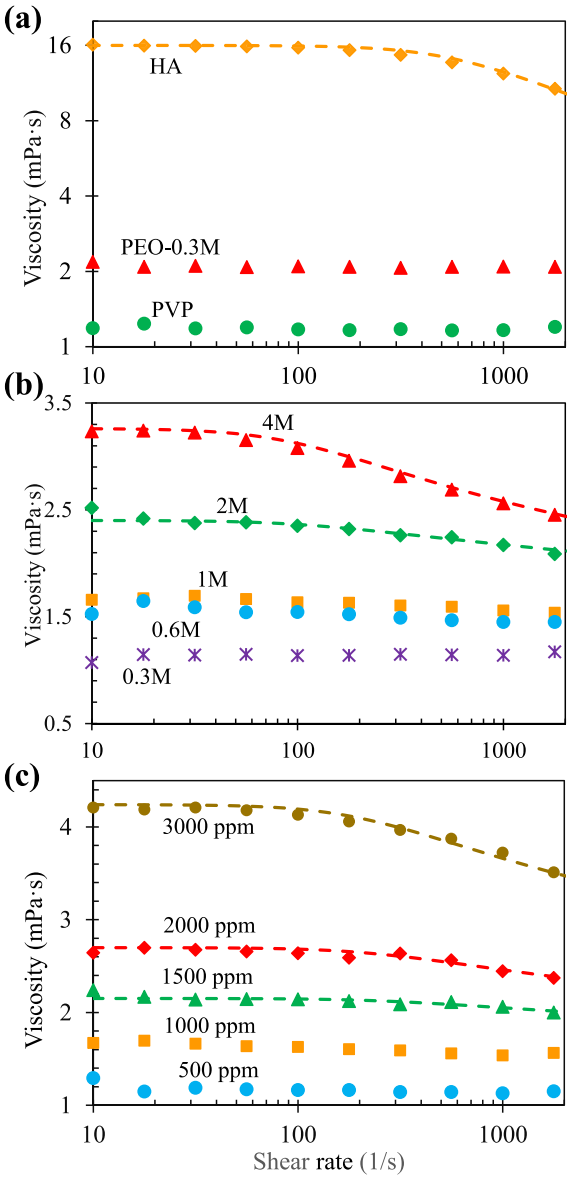

Fig. 2. Experimentally measured viscosity data (symbols) for the prepared polymer solutions: (a) 3000 ppm PEO, PVP, and HA solutions with similar molecular weights of around 0.3 MDa; (b) 1000 ppm PEO with varying molecular weights; (c) 1 MDa PEO at varying concentrations. The dashed lines on each plot represent the Carreau-model fitting of the viscosity data for the fluids exhibiting shear-thinning behaviors.

viscosity, λ_C is a time constant, and $\dot{\gamma}$ is the fluid shear rate. Note that the standard deviation of the fitted data, $\sigma = \sqrt{\sum (1 - measured/fitted)^2/N}$, was minimized (smaller than 2.5% for all cases) in the curve fitting, where N is the number of data points under consideration. The relaxation times of the prepared polymer solutions were found in the literature with appropriate scaling for the molecular weight and/or concentration effect if needed. Specifically, the relaxation times, λ, of the PEO solutions were estimated from the reported value of 1.5 ms for $c = 1000$ ppm, $M_w = 2$ MDa PEO solution, which was measured by Rodd et al. using capillary breakup extensional rheometry [64], via the following molecular-weight and concentration scaling [77],

$$\lambda \propto [\eta] M_w (c/c^*)^{0.65} \propto {M_w}^{2.073} c^{0.65} \tag{2}$$

where, $[\eta] = 0.072 {M_w}^{0.65}$ is the intrinsic viscosity and $c^* = 1/[\eta]$ is the overlap concentration for dilute PEO solutions. The relaxation time of 3000 ppm PVP solution was estimated from the reported value of 2.2 ms for 5% PVP solution, which was measured by Liu et al. using a small-amplitude oscillatory test [78], via the concentration scaling, $\lambda \propto c^{0.8}$, for a good solvent with solvent quality index of 0.6 [77]. The relaxation time of 3000 ppm, $M_w = 0.357$ MDa HA solution was estimated from the reported value of 0.11 ms for 700 ppm, $M_w = 0.9$ MDa HA solution, which was measured by Haward using an extensional flow oscillatory rheometer [79], via the following molecular-weight and concentration scaling,

$$\lambda \propto {M_w}^{1.8} c^{0.8} \tag{3}$$

The rheological properties for the prepared polymer solutions are summarized in Table 1.

2.2. Methods

To visualize the flow pattern in the constriction microchannel, fluorescent particles of 1 μm diameter (0.05% solids, Bangs Laboratories) were seeded into each of the prepared polymer solutions as well as water. A syringe pump (KD Scientific, Holliston, MA, USA) was used to drive the particle suspension through the channel in the range of flow rates from 1 to 70 ml/h. Prior to any test, the channel was primed with Tween 20 (0.5% vol. Thermo Fisher Scientific, Waltham, MA) for 5 min, which was found to help minimizing the particles sticking to the channel walls. The behavior of the tracing particles at the contraction-expansion region was recorded using an inverted fluorescent microscope (Nikon Eclipse TE2000U, Nikon Instrument) with a CCD camera (Nikon DS-Qi1Mc, Nikon Instrument, Lewisville, TX, USA). The exposure time and intensity of the incident blue light were tuned to obtain good streakline images at different flow rates. The obtained digital images were processed using the Nikon imaging software (NIS-Elements, Nikon Instrument, Lewisville, TX, USA).

The fluid inertial effect on the contraction and expansion flows at the constriction region of the microchannel is characterized using the local Reynolds number, Re,

$$Re = \frac{\rho V D_h}{\eta(\bar{\dot{\gamma}})} = \frac{2\rho Q}{\eta(\bar{\dot{\gamma}})(w+h)} \tag{4}$$

where ρ is the fluid density assumed equal to the density of the solvent (i.e., DI water) for dilute polymer solutions, $V = Q/hw$ is the speed corresponding to the flow through the constriction with Q being the volumetric flow rate, h the channel height and w the constriction width, $D_h = 2hw/(w+h)$ is the hydraulic diameter of the constriction, and $\eta(\bar{\dot{\gamma}})$ is the fluid viscosity estimated at the characteristic shear rate across the constriction width, i.e., $\bar{\dot{\gamma}} = 2V/w$. The fluid elasticity effect is characterized by the Weissenberg number, Wi,

$$Wi = \lambda \bar{\dot{\gamma}} = \frac{2\lambda Q}{w^2 h} \tag{5}$$

The elasticity number, El, which is defined as the ratio of the Weissenberg number to the Reynolds number, measures the relative importance of the elastic stress over the inertial stress,

$$El = \frac{Wi}{Re} = \frac{\lambda \eta(\bar{\dot{\gamma}})(w+h)}{\rho w^2 h} \tag{6}$$

The estimated value of El for each prepared fluid is presented in Table 1 for the flow rate of 10 ml/h, at which the calculated shear rate is 63131.3 s^{-1}. For the ease of description, we regard a fluid as weakly viscoelastic for $0 < El < 1$, mildly elastic for $1 \leq El < 10$, and strongly elastic for $El \geq 10$. We admit that the estimated values of Wi and El are probably not very accurate for the tested polymer solutions because of the lacking of the experimental data for the fluid relaxation time. This approximation is, however, not expected to change the overall trend that we will report in the next section for at least the various PEO

Table 1
Rheological properties of the prepared polymer solutions. The elasticity number, *El*, was estimated at the flow rate of 10 ml/h for all the fluids.

Polymer	M_w(MDa)	c(ppm)	λ(ms)	η_0(mPa·s)	η_∞(mPa·s)	λ_C(s)	n	*El*
PVP	0.36	3000	0.23	1.18	1.18	-	≈1	0.29
HA	0.357	3000	0.067	16	1.5	0.0018	0.62	0.33
PEO	0.3	3000	0.06	2.09	2.09	-	≈1	0.14
	0.3	1000	0.03	1.14	1.14	-	≈1	0.04
	0.6	1000	0.12	1.5	1.5	-	≈1	0.19
	1	1000	0.36	1.62	1.62	-	≈1	0.63
	2	1000	1.50	2.4	1.5	0.01	0.85	3.04
	4	1000	6.31	3.26	1.9	0.013	0.73	14.73
	1	500	0.30	1.15	1.15	-	≈1	0.37
	1	1500	0.46	2.15	1.4	0.004	0.90	0.92
	1	2000	0.56	2.7	1.6	0.0045	0.84	1.26
	1	3000	0.73	4.2	2.2	0.0052	0.80	2.29

solutions. The fluid shear-thinning effect is characterized by the power-law index, n, in Table 1, from which we notice that our dilute polymer solutions exhibit negligible to weak shear thinning effects with $0.75 \leq n < 1$ except the salt-free HA and 4 MDa PEO solutions that are both mildly shear thinning with $0.5 \leq n < 0.75$. In addition, the growth of the fluid vortices formed in the expansion and/or contraction flow is characterized by the dimensionless vortex length, $\chi_L = L_v/W$, where the vortex length, L_v, is measured directly from the experimental images and W is the width of the microchannel.

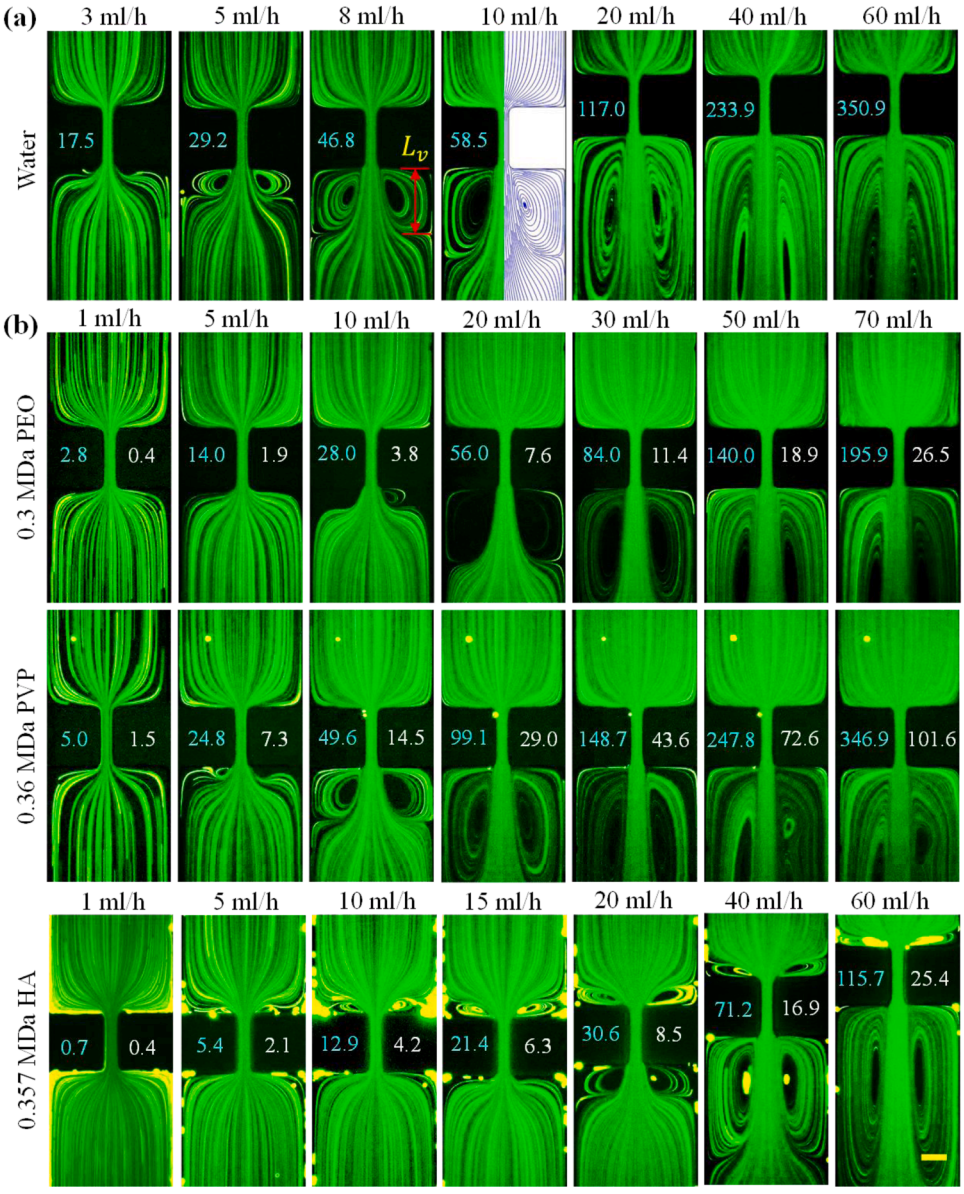

Fig. 3. Downward flows of Newtonian water (a) and viscoelastic solutions of 3000 ppm PEO, PVP and HA polymers with similar molecular weights of $M_w \approx 0.3$ MDa (b) through the constriction microchannel. The numbers labeled on the left and right sides of the channel constriction on each image indicate the corresponding Reynolds and Weissenberg numbers, respectively. The right half of the middle image in (a) shows the simulated fluid streamlines of water flow under the experimental conditions. The dimension, L_v, highlighted on the image in (a) measures the fluid vortex length. The scale bar on the right-most image in the last row represents 100 μm.

3. Results and discussions

3.1. Effect of polymer type

We tested the solutions of 3000 ppm PEO, PVP and HA polymers with similar molecular weights, $M_w \approx 0.3$ MDa, for the effect of polymer type on the flow in the constriction microchannel. These solutions exhibit a roughly equally weak elasticity with $El \sim 0.2$. However, as these polymers have different physical properties (e.g., contour length, coil size, etc.), the rheological properties of their aqueous solutions (e.g., viscosity, relaxation time, etc.) should also differ. In practice, the PEO and PVP solutions are both like Boger-like fluids [80] with negligible shear thinning while the HA solution is mildly shear thinning ($n = 0.62 < 0.75$). We also tested the flow of DI water (i.e., 0 ppm polymer) in the same microchannel as the control experiment. Fig. 3 shows the tracing particle streaklines in these fluids for flow rates of up to 70 ml/h. Like the purely inertial flow of water in Fig. 3(a), the expansion flow separation in each of the polymer solutions in Fig. 3(b) initiates with the symmetric lip vortices under a value of around $Re = 20$, which grow in both the sideway and along the length of the channel with the increase of *Re*. However, a little delayed formation of these vortices in the PEO flow is perhaps associated with the larger-magnitude of stretching or deformation of the flexible coils of the PEO polymer. Thus, despite the similar contour lengths, polymer concentrations, and time scales of the relaxation processes, the PEO molecules can expand and consequently suppress the inertial effects more at the expansion part compared to the relatively rigid PVP or HA molecules. Once the lip vortices reach the salient corners of the expansion walls, they continue to grow only in the primary flow direction. Such stable corner vortices in the expansion flow of water are found in Fig. 3(a) to match the numerically predicted fluid streamlines from a three-dimensional model in COMSOL® with the regular Navier-Stokes and continuity equations.

However, the three types of polymer solutions exhibit different behaviors in their contraction flows as viewed from the images in Fig. 3(b). The shear-thinning HA solution shows the development of small vortices in contrast to the no vortices at all in the non-shear-thinning PVP and PEO solutions. Small lip vortices first form in the HA solution at around $Re = 5.4$ (5 ml/h) on the re-entrant corners of the constriction and then grow on to reach the salient corners of the contraction walls at around $Re = 21.4$ (15 ml/h). The mild shear thinning effect present in the HA solution results in the formation of these steady symmetric vortices in the contraction flow, which are rather absent in constant-viscosity elastic flows through such structures, in compliance with our earlier observations in the contraction-flow of PAA and XG solutions through a similar planar constriction geometry [72]. Their size, however, does not grow much along the channel length like what we have observed in the strongly shear-thinning PAA and XG solutions [72]. This may be because the fluid shear thinning effect of the HA solution is not strong enough to dominate its inertial effect at higher values of *Re*. The short chain of HA polymers (as compared to those of the PAA and XG solutions) may also contribute to this behavior, which requires further studies. There are no such events other than the regular symmetric streamlines in the contraction flow of the PVP solution for the range of *Re* tested. Comparing it to the flow of Newtonian water, the viscoelastic PVP solution shows similar starting *Re* for the lip vortices and resembling development of them in size and appearance with the increase in *Re*. This is consistent with our recent observation of 5% PVP solution in a similar contraction-expansion microchannel [72]. In contrast, the contraction flow of the roughly equally elastic PEO solution shows weak bending streamlines at the salient corners starting under the highest flow rate of 70 ml/h ($Re = 195.9$) in our test. This may be a consequence of the dissimilar structures between the PVP and PEO polymers, which again requires further studies.

3.2. Effect of polymer molecular weight

For the effect of polymer length, we tested the solutions of 1000 ppm PEO with the molecular weight ranging from 0.3 MDa to 0.6 MDa, 1 MDa, 2 MDa and 4 MDa in the constriction microchannel. The first three solutions are all weakly elastic ($El < 1$) with negligible shear thinning. The 2 MDa PEO solution is a mildly elastic ($1 < El = 3.04 < 10$ at 10 ml/h) and a weakly shear thinning ($n = 0.85 > 0.75$) fluid. The 4 MDa PEO solution becomes strongly elastic ($El = 14.73 > 10$ at 10 ml/h) and mildly shear thinning ($n = 0.73 < 0.75$) (see Table 1). Fig. 4 shows the flow patterns at the contraction-expansion regions in these solutions. For the expansion flow, the vortex developments in the two lowest molecular-weight solutions, i.e., 0.3 MDa and 0.6 MDa, are both analogous to the purely inertial flow of water in Fig. 3(a), where the expansion flow vortices start from lip vortices and grow into large corner vortices extending downstream with increasing flow rates. Moreover, the size of these vortices are also comparable between the two solutions at similar values of *Re*. Increasing the molecular weight to 1 MDa makes the fluid vortices in the expansion flow start from the salient corners of the expansion walls at around $Re = 72.2$ (20 ml/h). This phenomenon seems to be associated with the comparable fluid elasticity and inertia effects in the 1 MDa PEO solution with $El = 0.63 \sim 1$. However, as no such salient-corner vortices have been observed in the strongly more elastic 5% PVP (0.36 MDa) solution ($El = 17.2$) in our recent work [72], we speculate it is probably mainly the consequence of the greater extensional stretching and re-orientation of the longer PEO polymer. These vortices grow with the increase of *Re* both inward from the salient corners to the channel center and downward following the flow. Further increasing the molecular weight to 2 MDa and 4 MDa causes the bending of fluid streamlines in the expansion flow at an earlier stage, but suppresses the expansion-flow vortices to a point of complete absence.

The contraction flow pattern of 0.3 MDa PEO solution maintains a good similarity with that of the purely inertial fluid water. No bending or vortices are found before the channel constriction in Fig. 4 as far as the flow rates are concerned. With the increase of molecular weight to 0.6 MDa and 1 MDa, a similar bending of fluid streamlines like that in Fig. 3 (b) for 3000 ppm, 0.3 MDa PEO solution is observed when *Re* reaches 155.9 (40 ml/h) and 54.1 (15 ml/h, not shown in Fig. 4), respectively. Note that both these values of *Re* are smaller than that in the 3000 ppm, 0.3 MDa PEO solution, $Re = 195.9$ (70 ml/h), because of the longer polymer chains in the 0.6 MDa and 1 MDa PEO solutions. When the molecular weight is increased to 2 MDa and 4 MDa, there is a single vortex forming at one side in the stagnant salient corner of the contraction part shortly after the appearance of streamline bending. This phenomenon is speculated to be associated with the increasing shear thinning effect in these two highest molecular-weight PEO solutions. The size of the single corner vortex increases with the increasing value of *Re* in both solutions. Its position, however, remains stably at the same side of the contraction after the formation, in contrast to the bistable phenomenon reported by Rodd et al. [64]. At an even higher value of *Re*, which is 162.9 (50 ml/h) for 2 MDa and 69.5 (25 ml/h) for 4 MDa, the status changes from a single corner vortex to asymmetric corner vortices with another smaller vortex formed in the opposite corner. However, this asymmetric state is unstable as the two vortices jump from one side to another of the contraction part at random intervals, which is different from the quasi-stable symmetric or asymmetric state reported by Rodd et al. [64]. It even becomes chaotic in the 4 MDa PEO solution at flow rates higher than 40 ml/h. Such unstable upstream eddies were reported by Browne et al. [81] to occur in an inertialess ($Re \ll 1$) flow of 18 MDa PAA solution through a single pore-throat. The stronger influence of the enhanced fluid elasticity and as well the reorientation and tumbling of longer polymer chains in the constriction region may have caused the observed flow pattern changes with the increasing molecular weight.

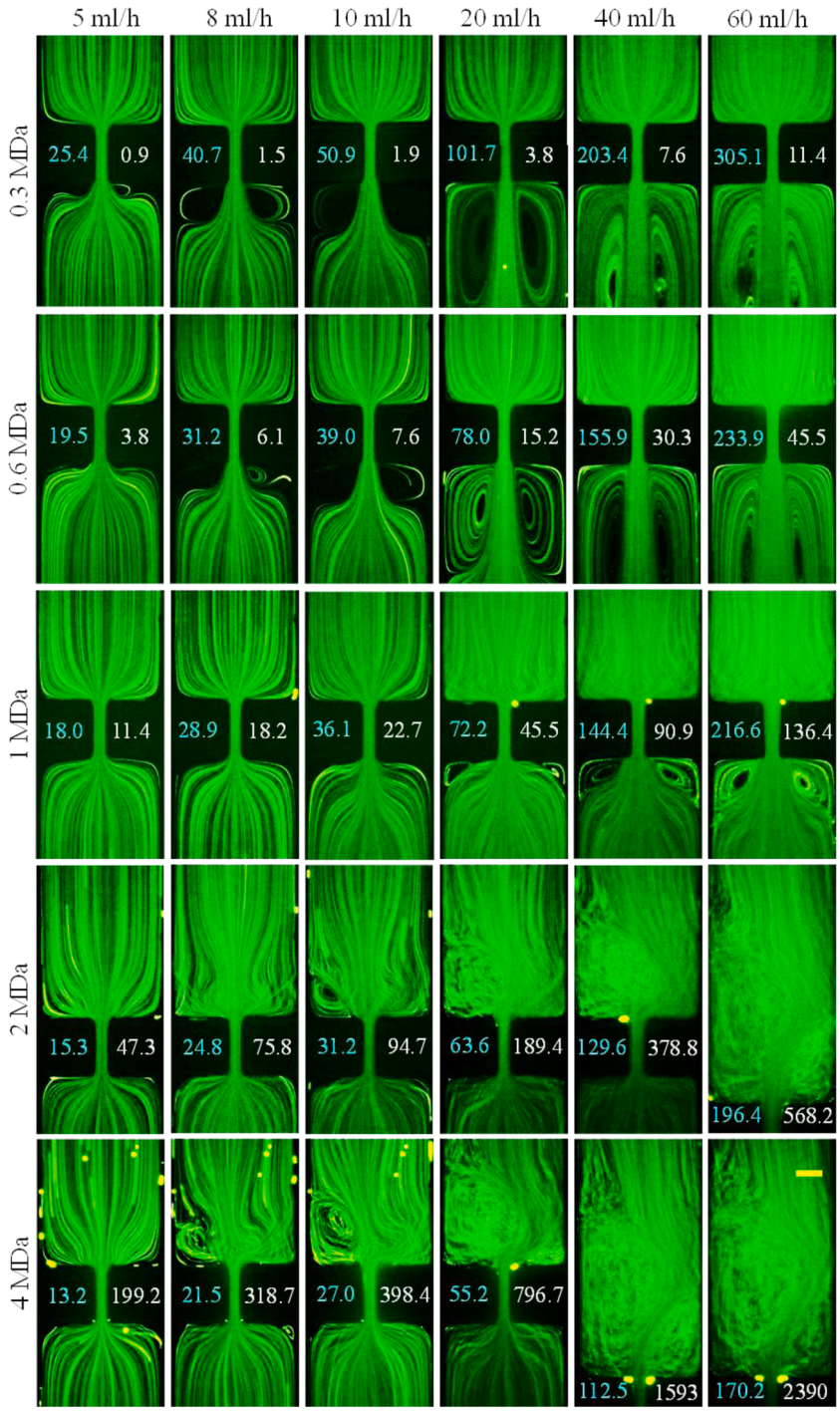

Fig. 4. Downward flows of viscoelastic solutions of 1000 ppm PEO with molecular weights ranging from 0.3 MDa to 4 MDa through the constriction microchannel in a range of flow rates. The numbers labeled on the left and right sides of the channel constriction on each image indicate the corresponding Reynolds and Weissenberg numbers, respectively. The scale bar on the bottom-right image represents 100 μm.

3.3. *Effect of polymer concentration*

We tested the solutions of 1 MDa PEO at 500 ppm, 1000 ppm, 1500 ppm, 2000 ppm and 3000 ppm for the effect of polymer concentration on the flow in the constriction microchannel. These fluids are negligibly to weakly shear thinning ($0.75 \leq n < 1$) and exhibit a weak-to-mild elasticity with the elasticity number, *El*, on the order of 1. Fig. 5 shows the flow patterns in these PEO solutions at the contraction-expansion region, which exhibits a similar development to the cases of increasing polymer molecular weights in Fig. 4. For the expansion flow, the overall trend observed is the elastic suppression of the fluid inertia-induced vortices with the increase in polymer concentration. In the solution with the lowest PEO concentration of 500 ppm, the vortex growth pattern is similar to water in Fig. 3(a). However, the inertial disturbances to the expansion flow initiate at around $Re = 25$, which is delayed than in the flow of water. Moreover, the length of the expansion-flow corner vortices exhibits an interesting non-monotonic trend with the increase of *Re*. This should be attributed to the competition of the fluid inertia (which promotes the vortex size) and elasticity (which suppresses the vortex size) effects. With the increase of PEO

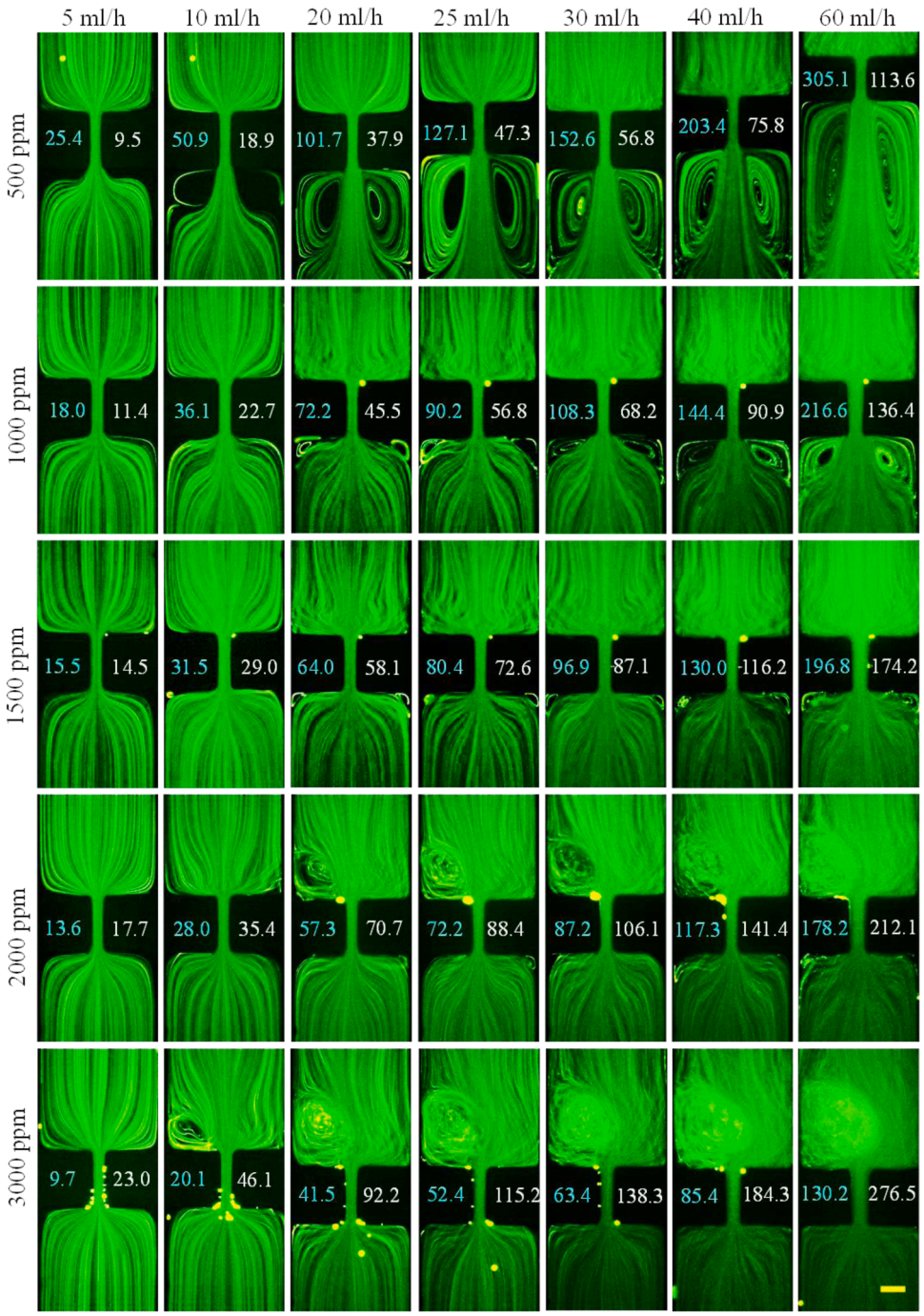

Fig. 5. Downward flows of 1 MDa PEO solutions having different concentrations in the constriction microchannel. The numbers labeled on the left and right sides of the channel constriction on each image indicate the corresponding Reynolds and Weissenberg numbers, respectively. The scale bar on the bottom-right image represents 100 μm.

concentration to 1000 ppm and 1500 ppm, the initiating location of the expansion-flow vortices is suppressed from being at the re-entrant lips and shifted to the salient corners of the expansion walls. For the 2000 ppm and 3000 ppm flows, there are no vortices but bending of streamlines for as far as the highest flow rate is concerned because of the strong fluid elasticity effect.

For the contraction flow, the onset of elastic disturbances occurs at $Re = 152.6$ (30 ml/h) in the lowest PEO ($M_w = 1$ MDa) concentration of 500 ppm. This starting value of *Re*, which is comparable to that in the 1000 ppm, 0.6 MDa PEO solution ($Re = 155.9$ at 40 ml/h) in Fig. 4, decreases for the higher concentration solutions of 1000 ppm and 1500 ppm as the diverging streamlines are observed in them at *Re* as early as 54.1 (15 ml/h) and 31.5 (10 ml/h), respectively. These diverging streamlines grow in intensity with the rise in *Re* but remain approximately symmetric for the rest of the tested flow rates. However, an increased concentration of 2000 ppm renders the diverging streamlines, which start developing at $Re < 28.0$ (10 ml/h), to collapse into a single vortex on one side near the salient corner of the contraction under higher flow rates. The transition from the diverging streamlines to the single vortex pattern takes place at around $Re = 57.3$ (20 ml/h), and the flow stays in this regime till the end of our tested cases ($Re = 178.2$ at 60 ml/h) for the flow of 2000 ppm PEO solution. These observed phenomena may be attributed to the greater normal stress differences in the flow of higher concentration solution with a larger elasticity. The

increase in fluid shear thinning may also have played a part in the formation of vortices in the contraction flow of 2000 ppm, 1 MDa PEO solution, like those in the 1000 ppm, 2 MDa and 4 MDa PEO solutions (Fig. 5). Further increasing the PEO concentration to 3000 ppm shifts the flow transitions to an even smaller value of *Re*. The single corner vortex state is maintained in both 2000 ppm and 3000 ppm PEO solutions for the whole range of tested flow rates (up to 60 ml/h). Its size increases continuously with the increasing value of *Re*, similar to that of the single vortex in 2 MDa and 4 MDa PEO solutions (Fig. 5).

3.4. Summary of flow regimes

A summary of the observed expansion flow regimes for the tested polymer solutions and water in the constriction microchannel is plotted in the $Re - Wi$ space in Fig. 6. As the Newtonian water flow (assigned a constant small Weissenberg number, $Wi = 0.1$, for the purpose of graphing) is observed to exhibit lip vortices near the re-entrant corners of the expansion walls at around $Re = 20$ in both the experiment and simulation, we highlight this *Re* on the plot as the start of the flow regime that fluid inertia plays a significant role. Regarding fluid viscoelasticity, we find it useful to divide the $Re - Wi$ space into three regimes based on the value of the elasticity number, *El*. The polymer solutions with $El < 0.5$ (estimated at 10 ml/h, see Table 1) show a similar flow development to that of water because of the dominant inertial effect over the elasticity effect. Specifically, the disturbances to the expansion flow of 500 ppm PEO-1M, 1000 ppm PEO-0.6M, 1000 ppm and 3000 ppm PEO-0.3M, 3000 ppm PVP and HA solutions all start with small lip vortices and then develop into stable corner vortices with the increase of *Re*. For the more viscoelastic polymer solutions with $El < 1.0$, the expansion flow vortices instead initiate at the salient corners. This transition should be associated with the comparable fluid elasticity and inertial effects in 1000 ppm and 1500 ppm PEO-1M solutions. For those polymer solutions with $El > 1.0$, the fluid inertia-induced expansion flow vortices are completely blocked by the strong elasticity effect. Only diverging streamlines are observed in 1000 ppm PEO-4M, 1000 ppm PEO-2M, 3000 ppm and 2000 ppm PEO-1M solutions.

Fig. 7 presents a summary of the observed contraction flow regimes for the tested polymer solutions in the $Re - Wi$ plot, where the whole space is divided into four regimes based on the value of *El*. Similar to the Newtonian water flow, no disturbances to the contraction flow are observed in 1000 ppm PEO-0.3M solution because of the insignificant fluid elasticity effect at $El < 0.1$. However, the contraction flow of 3000 ppm PVP solution also resembles that of water despite its $El = 0.29$. This observation is backed up by our recent study of 5% PVP solution with $El > 10$ in a similar constriction microchannel [72], which may be associated with its particular polymer structure and requires further studies. For the polymer solutions with $0.1 < El < 1.0$, symmetric diverging streamlines occur in the contraction flow if the Weissenberg number is large enough. Moreover, the greater *El* renders the diverging streamlines to start at a smaller Reynolds number. This flow regime covers 1500 ppm, 1000 ppm and 500 ppm PEO-1M, 1000 ppm PEO-0.6M, and 3000 ppm PEO-0.3M solutions. The only exception is 3000 ppm HA solution with $El = 0.33$, where first lip and then corner vortices are induced in its contraction flow by the fluid shear thinning effect. For the polymer solutions with $1.0 < El < 2.5$, which include 3000 ppm and 2000 ppm PEO-1M solutions, diverging streamlines can collapse into a single corner vortex when *Wi* is above a certain value. Further increasing the value of *El* to above 2.5 forces the contraction flow to change from a single vortex to unstable asymmetric vortices in 1000 ppm PEO-2M and PEO-4M solutions when *Wi* (or equivalently *Re*) becomes sufficiently high.

3.5. Summary of vortex development

Vortex development in the tested polymer solutions is quantified by the measured length of stable vortex, L_v [highlighted on the image in Fig. 3(a)], in the contraction and/or expansion part of the constriction microchannel. Fig. 8 shows the normalized vortex length, $\chi_L = L_v/W$, against *Re* in the expansion flow. As viewed from the highlighted values of *El* on the plot, the curves for the polymer solutions with $El < 0.35$ (including 1000 ppm and 3000 ppm PEO-0.3M, 1000 ppm PEO-0.6M, 3000 ppm PVP and HA solutions) almost coincide with that of the purely inertial vortices in water, illustrating an increasingly larger vortex with the increase of *Re*. The slight discrepancy among the curves is perhaps caused by the experimental error in the measurement of fluid viscosity or vortex length. For 500 ppm PEO-1M solution with $El = 0.37$, lip-initiated corner vortices are still available in the expansion flow. Their length, however, reaches a local maxima at around $Re = 127.1$ (at 25 ml/h) and starts increasing again after this point without any anomaly. This phenomenon may be associated with the elastic disturbances to the contraction flow that initiate at $Re = 152.6$ (at 30 ml/h) in the form of bending streamlines. For 1000 ppm and 1500 ppm PEO-1M solutions with $El > 0.5$, only corner-initiated vortices are observed (see Fig. 6). Their length becomes significantly smaller than that of the

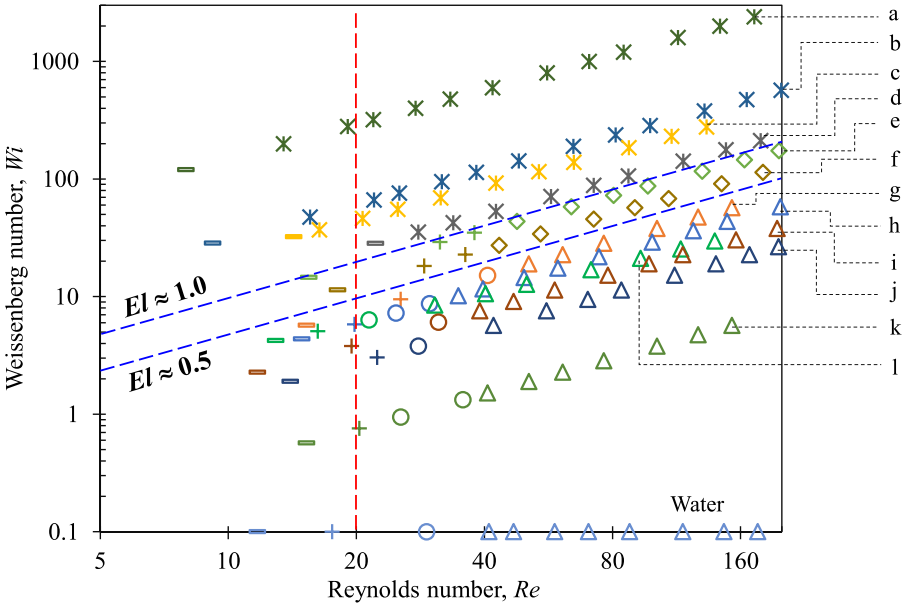

Fig. 6. Summary of the flow regimes in the $Re - Wi$ space for the expansion flow of viscoelastic polymer solutions (a: 1000 ppm PEO-4M; b: 1000 ppm PEO-2M; c: 3000 ppm PEO-1M; d: 2000 ppm-1M; e: 1500 ppm PEO-1M; f: 1000 ppm PEO-1M; g: 500 ppm PEO-1M; h: 3000 ppm PVP; i: 1000 ppm PEO-0.6M; j: 3000 ppm PEO-0.3M; k: 1000 ppm PEO-0.3M; l: 3000 ppm HA) and Newtonian water (the Weissenberg number is assumed to be 0.1 for the purpose of graphing) in the constriction microchannel: dashes for undisturbed flows; crosses for lip bending streamlines; circles for lip vortices; triangles for lip-initiated corner vortices; diamonds for corner-initiated vortices; asterisks are for bending and diverging streamlines. The vertical dashed-line at $Re = 20$ marks the transition to the flow regime where the fluid inertia-induced flow disturbances start occurring at the re-entrant corners. The other two straight dashed-lines highlight the transitions from the lip-initiated corner vortices to the corner-initiated vortices at $El \approx 0.5$ and to the vortex-free bending streamlines at $El \approx 1.0$.

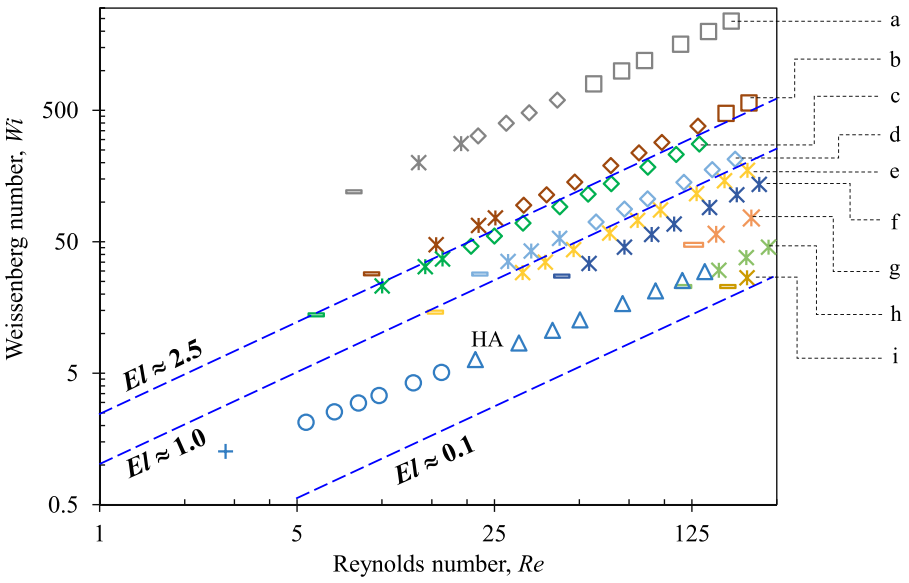

Fig. 7. Summary of the flow regimes in the $Re - Wi$ space for the contraction flow of viscoelastic polymer solutions (a: 1000 ppm PEO-4M; b: 1000 ppm PEO-2M; c: 3000 ppm PEO-1M; d: 2000 ppm-1M; e: 1500 ppm PEO-1M; f: 1000 ppm PEO-1M; g: 500 ppm PEO-1M; h: 1000 ppm PEO-0.6M; i: 3000 ppm PEO-0.3M) in the constriction microchannel: dashes for undisturbed flows; crosses for lip bending streamlines; circles for lip vortices; triangles for lip-initiated corner vortices; asterisks are for bending and diverging streamlines; diamonds for single corner vortices; squares for asymmetric corner vortices. The three straight dashed-lines highlight the transitions from the undisturbed flow to the diverging streamlines at $El \approx 0.1$, to the single corner vortices $El \approx 1.0$, and to the asymmetric corner vortices at $El \approx 2.5$.

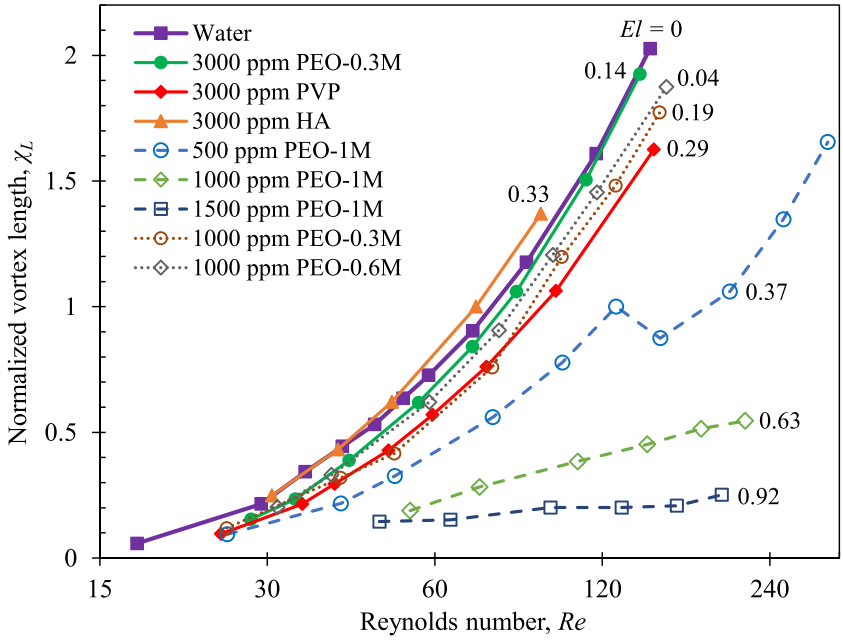

Fig. 8. Normalized vortex length, $\chi_L = L_v/W$, against the Reynolds number, Re, for the expansion flow of viscoelastic polymer solutions and Newtonian water in the constriction microchannel. The estimated value of the elasticity number, El, at the flow rate of 10 ml/h is highlighted for each fluid.

inertial vortices and decreases with the increasing polymer concentration. It, however, increases with the rise of Re in both solutions because of the enhanced inertial effect though to a much smaller extent than that of the inertial vortices. No expansion flow vortices are observed in the polymer solutions with $El > 1.0$.

Fig. 9 shows the normalized vortex length, χ_L, against Re in the contraction flow of the constriction microchannel. Only five of the tested polymer solutions exhibit vortices, among which one is the 3000 ppm HA solution with $El = 0.33$ and all the others are PEO solutions with $El > 1.0$. The fluid shear thinning-induced symmetric corner vortices in the contraction flow of the HA solution are much smaller than those of the fluid inertia-induced expansion flow vortices (see Fig. 8). Moreover, they exhibit a first increasing and then decreasing trend with the transition occurring at around $Re = 50$ because of the increasingly dominant inertial effect over the shear thinning effect. The contraction flow vortices in the four PEO solutions (all in the regime of single vortices) are all significantly larger than those in the HA solution. Their sizes, however, all grow with the increase of Re, in distinct contrast to the non-monotonic variation in the HA solution. These observations may be attributed to both the stronger fluid elasticity and the longer polymer chains of the PEO solutions. It is also viewed from Fig. 9 that the onset of the contraction flow vortices in the PEO solutions moves ahead and their length grows with the increase of the polymer length or concentration. However, neither of these changes is a simple function of the elasticity number. This may be because only single vortices appear in the 2000 ppm and 3000 ppm PEO-1M solutions while asymmetric vortices are formed in the 1000 ppm PEO-2M and PEO-4M solutions.

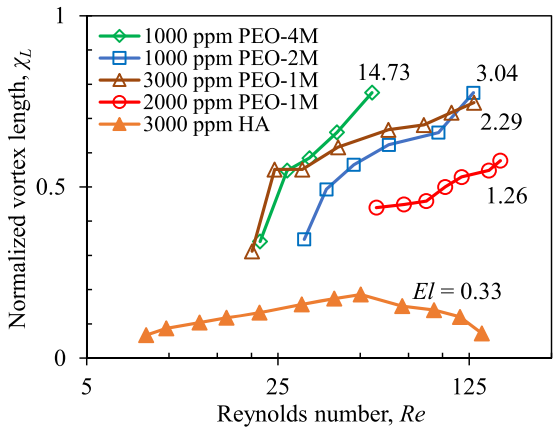

Fig. 9. Normalized vortex length, $\chi_L = L_v/W$, against the Reynolds number, *Re*, for the contraction flow of viscoelastic polymer solutions in the constriction microchannel. The estimated value of the elasticity number, *El*, at the flow rate of 10 ml/h is highlighted for each fluid.

3.6. Comparison with previous studies in similar geometries

There have been a good body of works on the flow of viscoelastic fluids, such as PAA [41,54,65,70,72,81], PAA-based Boger [68], PEO [38,42,52,64,66,72], PVP [72], Na-HA [71], XG [41,72], methylcellulose [82], polystyrene [83,84] and worm-like micelle [85] solutions, in a planar contraction-expansion microchannel. However, the majority of these studies paid attention to the contraction flow and provided little information on the expansion flow. Our study advances the understanding of the elasto-inertial effects on such flows in at least the following aspects: (a) We observe for the first time three different regimes in the expansion flow, which are the Newtonian water-like inertial vortices initiating from the lips in the polymer solutions with $El < 0.5$, the elasto-inertial vortices initiating at the salient corners in the solutions with $0.5 < El < 1.0$, and the vortex-free expansion flow in the solutions with $El > 1.0$; (b) Our value of *El* is varied from 0.04 (for 1000 ppm, 0.3 MDa PEO) to 14.73 (for 1000 ppm, 4 MDa PEO), which complements the previous studies [38,42,52,64,66,72] that exclusively used PEO solutions with $El > 1$. We observe in the contraction flow of PEO solutions with $0.1 < El < 1$ the onset of symmetric diverging streamlines if *Re* is large enough. No single or asymmetric vortices occur in these weakly elastic solutions even when the value of *Wi* reaches 136.4 for 1000 ppm 1 MDa PEO solution at 60 ml/h ($Re = 216.6$). In contrast, Rodd et al. [64] observed steady contraction flow vortices for $100 < Wi < 150$ in PEO solutions with $El > 1$; (c) We propose the use of *El* to divide the $Re - Wi$ space for both the contraction (Fig. 6) and expansion (Fig. 7) flows, in contrast to the critical *Wi* (or the Deborah number, *De*) that Rodd et al. [38,64] used for the contraction flow. As it is (nearly) independent of fluid kinematics, *El* may be viewed as a fluid property that is more convenient for uses. However, the value of *El* alone does not indicate the flow regime, which must be determined in conjunction with the value of *Wi* (or alternatively *Re*). Therefore, it will be very useful to identify a single dimensionless number, like the parameter, $M \equiv \sqrt{De \cdot Wi}$, developed by Pakdel and McKinley [86], for this purpose if available.

4. Conclusion

We have experimentally investigated the effects of polymer type, molecular weight, and concentration on viscoelastic fluid flows through a planar constriction microchannel. Changing the polymer type amongst PEO, PVP, and HA with similar molecular weights and concentrations does not affect the fluid inertia-induced vortices in the expansion flow, but causes completely different contraction flows because of their different molecular structures resulting in a diversion in the rheological properties amongst them in the larger length scales. Increasing the molecular weight of PEO polymer causes stronger disturbances to the streamlines and ultimately the formation of single or even asymmetric vortices in the contraction flow because of the enhanced fluid elasticity ($0.04 \le El \le 14.73$) and shear thinning ($1 \ge n \ge 0.73$) effects. The expansion flow encounters a greater resistance on flow separation and vortex formation as the polymer molecular weight increases. Increasing the polymer concentration of PEO solution also enhances the fluid elasticity and shear thinning effects, yielding similar influences on the flow regime to increasing the polymer molecular weight. Overall, we find that the fluid elasticity suppresses the fluid inertia-induced vortices in the expansion flow, and meanwhile draws instabilities into both the expansion and contraction flows in the form of bending streamlines. Interestingly in 500 ppm PEO solution, we have seen the inertial expansion-flow vortices decreasing in size when the streamline bending starts in the contraction flow. This phenomenon may indicate the dependence of the expansion and contraction flows as the effect of one may be propagated to the other through the polymer extensional, reorientational or relaxation process. We have also presented the observed flow patterns in each of the tested polymer solutions in the same dimensionless $Re - Wi$ and $Re - \chi_L$ parameter spaces. The elasticity number is found to play a determining role in both the flow regimes and the vortex development for at least the PEO solutions. It is hoped that our experimental data can stimulate more numerical studies (see, e.g., [11]) for a more accurate understanding of fluid rheological effects in polymer solution flows through porous media [28,59].

Declaration of Competing Interest

None.

Acknowledgements

This work was supported in part by China Scholarship Council (CSC) - Chinese Government Graduate Student Overseas Study Program (S.W. and L.S.), University 111 Project of China under grant number B12019 (L.Y.), Clemson University through a SEED grant (X.X.), and NSF under grant number CBET-1750208 (J.B.B.).

References

[1] K.S. Sorbie, Polymer-Improved Oil Recovery, 1st edn., Springer, Netherlands, XII, 1991, p. 359.
[2] J.F. Steffe, Rheological Methods in Food Process Engineering, Freeman Press, East Lansing, MI, USA, 1996.
[3] D.S. Roote, Technology Status Report In Situ Flushing, Ground-Water Remediation Technologies Analysis Center, 1998, pp. 1–164.
[4] D.V. Boger, Viscoelastic flows through contractions, Annual Rev. Fluid Mech. 19 (1987) 157–182.
[5] A. Lindner, Flow of complex suspensions, Phys. Fluid. 26 (2014), 101307.
[6] F.J. Galindo-Rosales, L. Campo-Deaño, P.C. Sousa, V.M. Ribeiro, M.S.N. Oliveira, M.A. Alves, F.T. Pinho, Viscoelastic instabilities in micro-scale flows, Exp. Therm. Fluid Sci. 59 (2014) 128–139.
[7] X. Shi, G.F. Christopher, Growth of viscoelastic instabilities around linear cylinder arrays, Phys. Fluids 28 (2016), 124102.
[8] A. Souliès, J. Aubril, C. Castelain, T. Burghelea, Characterisation of elastic turbulence in a serpentine micro-channel, Phys. Fluids 29 (2017), 083102.
[9] G. Yao, J. Zhao, H. Yang, M.A. Haruna, D. Wen, Effects of salinity on the onset of elastic turbulence in swirling flow, curvilinear microchannels, Phys. Fluids 31 (2019), 123106.
[10] P.G. Correa, J.R. Mac Intyre, J.M. Gomba, M.A. Cachile, J.P. Hulin, H. Auradou, Three-dimensional flow structures in X-shaped junctions: Effect of the Reynolds number, crossing angle, Phys. Fluids 31 (2019), 043606.
[11] S. Varchanis, C.C. Hopkins, A.Q. Shen, J. Tsamopoulos, S.J. Haward, Asymmetric flows of complex fluids past confined cylinders: a comprehensive numerical study with experimental validation, Phys. Fluids 32 (2020), 053103.
[12] R.B. Bird, R.C. Armstrong, O. Hassager, Dynamics of Polymeric Liquids, Wiley-Interscience, 1987, p. 1.
[13] R.G. Larson, Instabilities in viscoelastic flows, Rheolog. Acta 31 (1992) 213–263.
[14] S.J. Haward, G.H. McKinley, Instabilities in stagnation point flows of polymer solutions, Phys. Fluids 25 (2013), 083104.
[15] R.G. Larson, Flow-induced mixing, demixing and phase-transitions in polymeric fluids, Rheolog. Acta 31 (1992) 497–520.

[16] J.A. Pathak, D. Ross, K.B. Migler, Elastic flow instability, curved streamlines, mixing in microfluidic flows, Phys. Fluids 16 (2004) 4028–4034.
[17] H.Y. Gan, Y.C. Lam, N.T. Nguyen, K.C. Tam, C. Yang, Efficient mixing of viscoelastic fluids in a microchannel at low Reynolds number, Microfluid. Nanofluid. 3 (2007) 101–108.
[18] S.O. Hong, J.J. Cooper-White, J.M. Kim, Inertio-elastic mixing in a straight microchannel with side wells, Appl. Phys. Lett. 108 (2016) 13–17.
[19] G. D'Avino, F. Greco, P.L. Maffettone, Particle migration due to viscoelasticity of the suspending liquid and its relevance in microfluidic devices, Annu. Rev. Fluid Mech. 49 (2017) 341–360.
[20] X. Lu, C. Liu, G. Hu, X. Xuan, Particle manipulations in non-Newtonian microfluidics: a review, J. Colloid Interf. Sci. 500 (2017) 182–201.
[21] F. Tian, Q. Feng, Q. Chen, C. Liu, T. Li, J. Sun, Manipulation of bio-micro/nanoparticles in non-newtonian microflows, Microfluid. Nanofluid. 23 (2019) 68.
[22] M.K. Raihan, D. Li, A.J. Kummetz, L. Song, L. Yu, Vortex trapping and separation of particles in shear thinning fluids, Appl. Phys. Lett. 116 (2020), 183701.
[23] M.S.N. Oliveira, L.E. Rodd, G.H. McKinley, M.A. Alves, Simulations of extensional flow in microrheometric devices, Microfluid. Nanofluid. 5 (2008) 809–826.
[24] F.J. Galindo-Rosales, L. Campo-Deano, F.T. Pinho, E. van Bokhorst, P.J. Hamersma, M.S.N. Oliveira, M.A. Alves, Microfluidic systems for the analysis of viscoelastic fluid flow phenomena in porous media, Microfluid. Nanofluid. 12 (2012) 485–498.
[25] F.J. Galindo-Rosales, M.A. Alves, M.S.N. Oliveira, Microdevices for extensional rheometry of low viscosity elastic liquids: a review, Microfluid. Nanofluid. 14 (2013) 1–19.
[26] E.A. Gryparis, S.D. Gkormpatsis, K.D. Housiadas, R.I. Tanner, Viscoelastic planar elongational flow past an infinitely long cylinder, Phys. Fluids 31 (2019), 033104.
[27] A. Phan, D. Fan, A. Striolo, Fluid transport through heterogeneous pore matrices: Multiscale simulation approaches, Phys. Fluids 32 (2020), 101301.
[28] C.A. Browne, A. Shih, S.S. Datta, Pore-scale flow characterization of polymer solutions in microfluidic porous media, Small 16 (2020), 1903944.
[29] K. Walters, D.M. Rawlinson, On some contraction flows for Boger fluids, Rheol. Acta 21 (1982) 547–552.
[30] R.E. Evans, K. Walters, Flow characteristics associated with abrupt changes in geometry in the case of highly elastic liquids, J Non-Newton. Fluid Mech. 20 (1986) 11–29.
[31] K. Chiba, T. Sakatani, K. Nakamura, Anomalous flow patterns in viscoelastic entry flow through a planar contraction, J. Non-Newton. Fluid Mech. 36 (1990) 193–203.
[32] J.P. Rothstein, G.H. McKinley, Extensional flow of a polystyrene Boger fluid through a 4:1:4 axisymmetric contraction/expansion, J. Non-Newton. Fluid Mech. 86 (1999) 61–88.
[33] J.P. Rothstein, G.H. McKinley, The axisymmetric contraction-expansion: the role of extensional rheology on vortex growth dynamics and the enhanced pressure drop, J. Non-Newton. Fluid Mech. 98 (2001) 33–63.
[34] S. Nigen, K. Walters, Viscoelastic contraction flows: Comparison of axisymmetric and planar configurations, J. Non-Newton. Fluid Mech. 102 (2002) 343–359.
[35] M.A. Alves, P.J. Oliveira, F.T. Pinho, Benchmark solutions for the flow of Oldroyd-B and PTT fluids in planar contractions, J. Non-Newton. Fluid Mech. 110 (2003) 45–75.
[36] R.J. Poole, M.P. Escudier, Turbulent flow of viscoelastic liquids through an axisymmetric sudden expansion, J. Non-Newton. Fluid Mech. 117 (2004) 25–46.
[37] R.J. Poole, M.P. Escudier, A. Afonso, F.T. Pinho, Laminar flow of a viscoelastic shear-thinning liquid over a backward-facing step preceded by a gradual contraction, Phys. Fluid. 19 (2007), 093101.
[38] L.E. Rodd, J.J. Cooper-White, D.V. Boger, G.H. McKinley, Role of the elasticity number in the entry flow of dilute polymer solutions in micro-fabricated contraction geometries, J. Non-Newton. Fluid Mech. 143 (2007) 170–191.
[39] S. Gulatia, S.J. Muller, D. Liepmanna, Direct measurements of viscoelastic flows of DNA in a 2:1 abrupt planar micro-contraction, J. Non-Newton. Fluid Mech. 155 (2008) 51–66.
[40] S.C. Omowunmi, X.F. Yuan, Modelling the three-dimensional flow of a semi-dilute polymer solution in microfluidics-on the effect of aspect ratio, Rheolog. Acta 49 (2010) 585–595.
[41] P.C. Sousa, F.T. Pinho, M.S.N. Oliveira, M.A. Alves, Extensional flow of blood analog solutions in microfluidic devices, Biomicrofluid 5 (2011), 014108.
[42] T.J. Ober, S.J. Haward, C.J. Pipe, J. Soulages, G.H. McKinley, Microfluidic extensional rheometry using a hyperbolic contraction geometry, Rheolog. Acta 52 (2013) 529–546.
[43] J.E. López-Aguilar, H.R. Tamaddon-Jahromi, M.F. Webster, K. Walters, Numerical vs experimental pressure drops for Boger fluids in sharp-corner contraction flow, Phys. Fluids 28 (2016), 103104.
[44] S.J. Haward, J. Page, T.A. Zaki, A.Q. Shen, Phase diagram for viscoelastic Poiseuille flow over a wavy surface, Phys. Fluids 30 (2018), 113101.
[45] T. Tomkovic, E. Mitsoulis, S.G. Hatzikiriakos, Contraction flow of ionomers and their corresponding copolymers: ionic and hydrogen bonding effects, Phys. Fluids 31 (2019), 033102.
[46] C. Sasmal, Flow of wormlike micellar solutions through a long micropore with step expansion and contraction, Phys. Fluids 32 (2020), 013103.
[47] L.L. Ferrás, A.M. Afonso, M.A. Alves, J.M. Nóbrega, F.T. Pinho, Newtonian and viscoelastic fluid flows through an abrupt 1:4 expansion with slip boundary conditions, Phys. Fluids 32 (2020), 043103.
[48] P.R. Varges, B.S. Fonseca, P.R. de Souza Mendes, M.F. Naccache, C.R. de Miranda, Flow of yield stress materials through annular abrupt expansion–contractions, Phys. Fluids 32 (2020), 083101.
[49] S.A. White, A.D. Gotsis, D.G. Baird, Review of the entry flow problem: experimental and numerical, J. Non-Newton. Fluid Mech. 24 (1987) 121–160.
[50] M.A. Alves, P.J. Oliveira, F.T. Pinho, On the effect of contraction ratio in viscoelastic flow through abrupt contractions, J. Non-newton. Fluid Mech. 122 (2004) 117–130.
[51] M.S.N. Oliveira, P.J. Oliveira, F.T. Pinho, M.A. Alves, Effect of contraction ratio upon viscoelastic flow in contractions: the axisymmetric case, J. Non-Newton. Fluid Mech. 147 (2007) 92–108.
[52] L.E. Rodd, D. Lee, K.H. Ahn, J.J. Cooper-White, The importance of downstream events in microfluidic viscoelastic entry flows: consequences of increasing the constriction length, J. Non-Newton. Fluid Mech. 165 (2010) 1189–1203.
[53] P.C. Sousa, P.M. Coelho, M.S.N. Oliveira, M.A. Alves, Effect of the contraction ratio upon viscoelastic fluid flow in three-dimensional square–square contractions, Chem. Eng. Sci. 66 (2011) 998–1009.
[54] A. Lanzaro, X.F. Yuan, Effects of contraction ratio on non-linear dynamics of semi-dilute, highly polydisperse PAAm solutions in microfluidics, J. Non-Newton. Fluid Mech. 166 (2011) 1064–1075.
[55] J.E. López-Aguilar, M.F. Webster, H.R. Tamaddon-Jahromi, M. Pérez-Camacho, O. Manero, Contraction-ratio variation and prediction of large experimental pressure-drops in sharp-corner circular contraction-expansions–Boger fluids, J. Non-Newton. Fluid Mech. 237 (2016) 39–53.
[56] R.M. Matos, M.A. Alves, F.T. Pinho, Instabilities in micro-contraction flows of semi-dilute CTAB and CPyCl solutions: rheology and flow instabilities, Exp. Fluid. 60 (2019) 145.
[57] C.D. Meinhart, H. Zhang, The flow structure inside a microfabricated inkjet printhead, J. Microelectromech. Syst. 9 (2000) 67–75.
[58] A.C. Barbati, J. Desroches, A. Robisson, G.H. McKinley, Complex fluids and hydraulic fracturing, Annu. Rev. Chem. Biomol. Eng. 7 (2016) 415–453.
[59] A. Anbari, H.T. Chien, S.S. Datta, W. Deng, D.A. Weitz, J. Fan, Microfluidic model porous media: fabrication and applications, Small 14 (2018), 1703575.
[60] M. Daoud, J.P. Cotton, B. Farnoux, G. Jannink, G. Sarma, H. Benoit, R. Duplessix, C. Picot, P.G. de Gennes, Solutions of flexible polymers-neutron experiments and interpretation, Macromolecules 8 (1975) 804–818.
[61] W.W. Graessley, Polymeric Liquids & Networks: Structure and Properties, CRC Press, 2003.
[62] M. Rubinstein, R.H. Colby, Polymer Physics, Oxford University Press Inc., Oxford, U.K., 2003.
[63] A.V. Dobrynin, M. Rubinstein, Theory of polyelectrolytes in solutions and at surfaces, Prog. Polym. Sci. 30 (2005) 1049–1118.
[64] L.E. Rodd, T.P. Scott, D.V. Boger, J.J. Cooper-White, G.H. McKinley, The inertio-elastic planar entry flow of low-viscosity elastic fluids in micro-fabricated geometries, J. Non-Newton. Fluid Mech. 129 (2005) 1–22.
[65] A. Lanzaro, Z. Li, X.F. Yuan, Quantitative characterization of high molecular weight polymer solutions in microfluidic hyperbolic contraction flow, Microfluid. Nanofluid. 18 (2015) 819–828.
[66] Z. Li, X.F. Yuan, S.J. Haward, J.A. Odell, S. Yeates, Non-linear dynamics of semi-dilute polydisperse polymer solutions in microfluidics: A study of a benchmark flow problem, J. Non-Newton. Fluid Mech. 166 (2011) 951–963.
[67] E. Miller, J.J. Cooper-White, The effects of chain conformation in the microfluidic entry flow of polymer–surfactant systems, J. Non-Newton. Fluid Mech. 60 (2009) 22–30.
[68] L. Campo-Deañoa, F.J. Galindo-Rosales, F.T. Pinho, M.A. Alves, M.S.N. Oliveira, Flow of low viscosity Boger fluids through a microfluidic hyperbolic contraction, J. Non-Newton. Fluid Mech. 166 (2011) 1286–1296.
[69] D. Kawale, E. Marques, P.L.J. Zitha, M.T. Kreutzer, W.R. Rossen, P.E. Boukany, Elastic instabilities during the flow of hydrolyzed polyacrylamide solution in porous media: effect of pore-shape and salt, Soft Matt. 13 (2017) 765–775.
[70] E.M. Ekanem, S. Berg, S. De, A. Fadili, T. Bultreys, M. Rücker, J. Southwick, J. Crawshaw, P.F. Luckham, Signature of elastic turbulence of viscoelastic fluid flow in a single pore throat, Phys. Rev. E 101 (2020), 042605.
[71] R. Hidema, T. Oka, Y. Komoda, H. Suzuki, Effects of flexibility and entanglement of sodium hyaluronate in solutions on the entry flow in micro abrupt contraction-expansion channels, Phys. Fluids 31 (2019), 072005.
[72] P.P. Jagdale, D. Li, X. Shao, J.B. Bostwick, X. Xuan, Fluid rheological effects on the flow of polymer solutions in a contraction-expansion microchannel, Micromachines 11 (2020) 278.
[73] C.J. Pipe, G.H. McKinley, Microfluidic rheometry, Mech. Res. Commun. 36 (2009) 110–120.
[74] X. Hu, P.E. Boukany, O.L. Hemminger, L.J. Lee, The use of microfluidics in rheology, Macromol. Mat. Eng. 296 (2011) 308–320.
[75] S.J. Haward, Microfluidic extensional rheometry using stagnation point flow, Biomicrofluid 10 (2016), 043401.
[76] X. Lu, S. Patel, M. Zhang, S.W. Joo, S. Qian, A. Ogale, X. Xuan, An unexpected particle oscillation for electrophoresis in viscoelastic fluids through a microchannel constriction, Biomicrofluid 8 (2014), 021802.
[77] V. Tirtaatmadja, G.H. McKinley, J.J. Cooper-White, Drop formation and breakup of low viscosity elastic fluids: effects of molecular weight and concentration, Phys. Fluids 18 (2006), 043101.
[78] C. Liu, C. Xue, X. Chen, Shan L, Y. Tian, G. Hu, Size-based separation of particles and cells utilizing viscoelastic effects in straight microchannels, Anal. Chem. 87 (2015) 6041–6048.
[79] S.J. Haward, Characterization of hyaluronic acid and synovial fluid in stagnation point elongational flow, Biopolymers 101 (2014) 287–305.
[80] D.F. James, Boger fluids, Annu. Rev. Fluid Mech. 41 (2009) 129–142.
[81] C.A. Browne, A. Shih, S.S. Datta, Bistability in the unstable flow of polymer solutions through pore constriction arrays, J. Fluid Mech. 890 (2020) A2.

[82] M.W. Collis, M.R. Mackley, The melt processing of monodisperse and polydisperse polystyrene melts within a slit entry and exit flow, J. Non-Newton. Fluid Mech. 128 (2005) 29–41.
[83] S.J. Haward, Z. Li, D. Lighter, B. Thomas, J.A. Odell, X. Yuan, Flow of dilute to semi-dilute polystyrene solutions through a benchmark 8:1 planar abrupt micro-contraction, J. Non-Newton. Fluid Mech. 165 (2010) 1654–1669.
[84] P.F. Salipante, S.E. Meek, S.D. Hudson, Flow fluctuations in wormlike micelle fluids, Soft Matter 14 (2018) 9020–9035.
[85] B.L. Micklavzina, A.E. Metaxas, C.S. Dutcher, Microfluidic rheology of methylcellulose solutions in hyperbolic contractions and the effect of salt in shear and extensional flows, Soft Matter 16 (2020) 5273–5281.
[86] P. Pakdel, G.H. McKinley, Elastic instability and curved streamlines, Phys. Rev. Lett. 77 (1996) 2459–2462.